Negative magnetization and inverse exchange bias effect induced by modulating the relative proportion of Mn in $Gd_2Co_{2-x}Mn_xO_6$ perovskites

Canglong Li,[1,*] Wenqian Yang,[1] Shuangshuang Zheng,[1] Godfrey Okumu Barasa,[2] Yang Qiu,[1] and Chunxu Bai[1,†]
[1]*Key Laboratory of Microelectronics and Energy of Henan Province, College of Physics and Electronic Engineering, Xinyang Normal University, Xinyang 464000, People's Republic of China*
[2]*Department of Physical Sciences, Jaramogi Oginga Odinga University of Science and Technology, Box 210, 40601 Bondo, Kenya*

(Received 7 December 2022; revised 23 May 2023; accepted 13 June 2023; published 28 June 2023)

The magnetic properties of $Gd_2Co_{2-x}Mn_xO_6$ by modulating the relative proportion of Mn are experimentally investigated in this paper. The experimental results indicated that an intrinsic effect of negative magnetization (NM) characterized by $M_{FC} < 0$ under moderate positive cooling fields H_{cool} was observed in the samples from $x = 1.1$ to 1.5. Magnetic field or temperature-assisted switching effects by manipulating the magnetization states from positive to negative and vice versa were realized with high repeatability, stability, and controllability, which exhibit promising applications in spintronic devices. More interestingly, an inverse exchange bias effect was observed below the compensation temperature T_{comp}. The experiment indicates that the inverse nature of exchange bias has the same origin as NM, which is attributed to the opposite alignment of the net ferromagnetic moments to the applied cooling field below the ferrimagnetic compensation point. In this paper, we provide a promising approach to trigger intriguing magnetic properties for future applications in spintronic devices by modulating the relative proportion of magnetic ions.

DOI: 10.1103/PhysRevB.107.214445

I. INTRODUCTION

The phenomenon of negative magnetization (NM) is defined as a crossover of direct-current magnetization from $+M$ to $-M$ under a positive magnetic field below magnetic ordering temperature, but it is not caused by diamagnetism [1]. Such an intriguing and unusual phenomenon has drawn great interest because of the two tunable states (positive and negative) of magnetization under applied magnetic field (H) and temperature (T) as well as the underlying physical mechanism. The H- or T−driven phenomenon has been found and investigated in several antiferromagnetic (AFM), ferromagnetic (FM), and ferrimagnetic (FIM) systems such as perovskite compounds of chromite/orthoferrite [2,3], spinel compounds [4–7], and rare-earth iron garnets [8,9]. As signified previously in $La_{1.5}Sr_{0.5}Co_{1-x}Fe_xMnO_6$ [10,11], as well as most recently in Er_2CoMnO_6 and Gd_2CoRuO_6 [12,13], the quaternary oxides with the empirical formula $R_2BB'O_6$ (R: rare-earth ions; B and B': transition metal ions) not only show the remarkable feature of NM but also simultaneously exhibit the inverse exchange bias effect, which could be ascribed to the mixed exchange coupling at the interface of ordered phase, antisite disordered phase, and adjacent magnetic clusters.

Double perovskites (DPs) $R_2BB'O_6$ have aroused renewed research interest because of their intriguing properties such as metamagnetism [14], magnetocaloric effect [15–17], and exchange bias [18,19] as well as NM [[10–13]. The crystal structure of the compounds depends on the crystallographic occupation of B and B'. The random arrangement of B/B' leads to orthorhombic structure with space group $Pbnm$ for the disordered state, while the alternating arrangement results in monoclinic $P2_1/n$ structure for the ordered state [20,21]. In contrast to the extensively studied La-based systems, there are relatively limited investigations on magnetic and electric properties of heavy rare-earth-based R_2CoMnO_6 DPs. The hopping of electrons from the half-filled orbital of the Jahn-Teller (JT) active ion Co^{2+} ($t_{2g}^5e_g^2$) to the vacant orbital of the JT nonactive ion Mn^{4+} ($t_{2g}^3e_g^0$) brings about FM superexchange interaction [22]. However, even in the ordered state, supplementary AFM interactions in the form of $Co^{2+}-O^{2-}-Co^{2+}$ and $Mn^{4+}-O^{2-}-Mn^{4+}$ are instigated due to the antisite disorder caused by the interchange of crystallographic positions between Co and Mn [23,24]. The defect is often encountered in DPs and consequently results in mixed valency due to the charge transfer between B and B'. Additionally, the magnetic ground state of R_2CoMnO_6 DPs is closely related to the R size since the Co−O−Mn bond angle/length can be significantly modified by the variation of the R size. For instance, La_2CoMnO_6 displays linear FM order along the c axis, while Lu_2CoMnO_6 possesses ↑↑↓↓ AFM configuration [25,26]. Therefore, coexistence of FM and AFM is reasonable to expect in DPs with R between La and Lu.

Gd_2CoMnO_6 belongs to the family of $R_2BB'O_6$ DPs, and it undergoes long-range FM order below the Curie point T_C (∼123 K) [20]. Some of the most recent first-principles calculations indicate that the spin channels of Gd_2CoMnO_6 display a band gap, so it shows correlation-driven insulator behavior [27,28]. A field-induced metamagnetic transition is detected at a lower temperature (∼115 K), and the transition is depressed in temperature for an external magnetic

*Authors to whom correspondence should be addressed: licanglong@xynu.edu.cn
†Authors to whom correspondence should be addressed: chunxu_bai@163.com

field [14]. Upon further decreasing the temperature to ∼43 K, a hump identified as AFM order is noticed, and it is attributed to the negative exchange coupling between Gd and Co/Mn sublattices [21,29]. In this paper, magnetic properties of $Gd_2Co_{2-x}Mn_xO_6$ compounds have been experimentally investigated by modulating the relative proportion of Mn to increase the antisite disorder. The research motivation is to improve the functional properties of the materials and also contribute to an in-depth understanding of the magnetic mechanisms behind the DPs. Based on the analyses of magnetization (magnetic susceptibility) as a function of temperature, magnetic field, and time, we discuss possible mechanisms of NM and the inverse exchange bias effect in $Gd_2Co_{2-x}Mn_xO_6$.

II. EXPERIMENTAL METHODS

By increasing the relative proportion of Mn in $Gd_2Co_{2-x}Mn_xO_6$ $(1.0 \leqslant x \leqslant 1.65)$, the polycrystalline samples were synthesized by a conventional solid-state reaction route as described previously [16,17]. The stoichiometric amounts of Gd_2O_3 (99.99%), CoO (99.9%), and $MnCO_3$ (99.95%) were mixed thoroughly and calcinated at 1000 °C in air for 24 h. Then the obtained powders were heated at 1200 °C for 24 h with intermediate grindings. Finally, the products were reground, pressed into discs with a thickness of 1 mm and a radius of 10 mm, and sintered at 1350 °C for 24 h with a cooling rate of 1° C/min. The crystal structure and phase purity of the prepared samples were identified by room-temperature x-ray powder diffraction with Cu-$K\alpha$ radiation (XRD, Smartlab-9, Rigaku, $\lambda = 1.5406$ Å). GSAS software was used to refine the XRD data by the Rietveld refinement. The charge states were detected by x-ray photoelectron spectrometer (XPS, Thermo Scientific, K-Alpha 0.5 eV) measurements. The magnetization measurements were carried out on a Quantum Design VSM magnetometer and a PPMS-DynaCool-9 T system.

III. RESULTS

The XRD patterns of $Gd_2Co_{2-x}Mn_xO_6$ $(1.0 \leqslant x \leqslant 1.65)$ are shown in Fig. 1(a). All the diffraction peaks can be indexed well with monoclinic $(1.0 \leqslant x \leqslant 1.4)$ or orthorhombic $(1.5 \leqslant x \leqslant 1.65)$ DPs. It suggests that the prepared samples are in single phase without impurity within the x-ray resolution. The enlarged view around the main peak displayed in Fig. 1(b) shows the detail of the Bragg positions, the obvious peak shift indicating the change of the crystal cell. To obtain the structural information, Rietveld analysis is carried out, and the refined XRD patterns of two representative samples at $x = 1.2$ and 1.4 are depicted in Figs. 1(c) and 1(d), respectively. The observed (Iobs.) intensity profile along with the calculated (Ical.) fit presents a high match with a small difference (Idiff.).

The refined lattice parameters a, b, c, and V together with β are summarized in Fig. 2, with reliability factors R_{wp} (1.32–4.35), R_P (0.94–3.01), and χ^2 (1.71–3.79). Apparently, an increased Mn content x $(1.0 \leqslant x \leqslant 1.65)$ results in the increase in lattice constants a and b and consequently unit cell volume V. In contrast, an increased Mn content lowers the lattice constant c. The expansion of the unit cell is mainly due

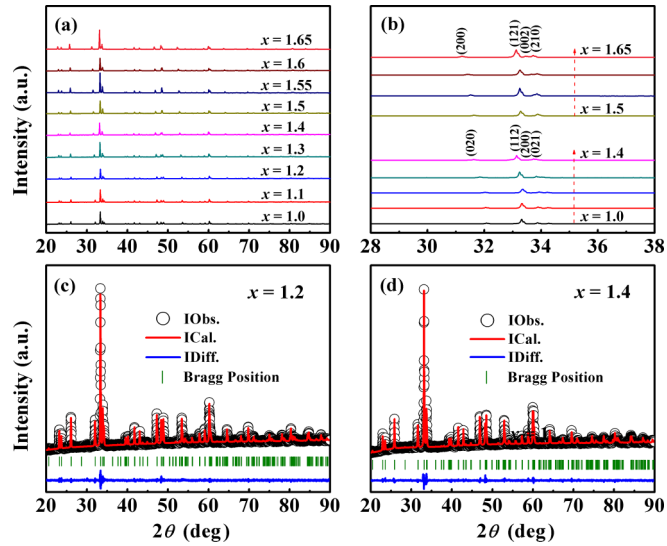

FIG. 1. (a) Room-temperature powder x-ray diffraction (XRD) patterns of $Gd_2Co_{2-x}Mn_xO_6$ $(1.0 \leqslant x \leqslant 1.65)$. (b) Enlarged view of the main peak. Refined XRD patterns for the samples at (c) $x = 1.2$ and (d) $x = 1.4$.

to the larger radius of the excess Mn ions with smaller atomic number than Co ions. The change of ion radius caused by charge transfer between Co and Mn ions could be the reason why the variation of sample lattice parameters deviates from Vegard's law [30]. The mixed valence of Co and Mn ions was characterized by XPS displayed in Figs. S1(a) and S1(b) in the Supplemental Material [31], respectively. This nonlinear change of lattice constant has also been reported in recent literature on DPs [27]. According to the crystallographic angle β, it is noticeable that the crystal structure can be classified as

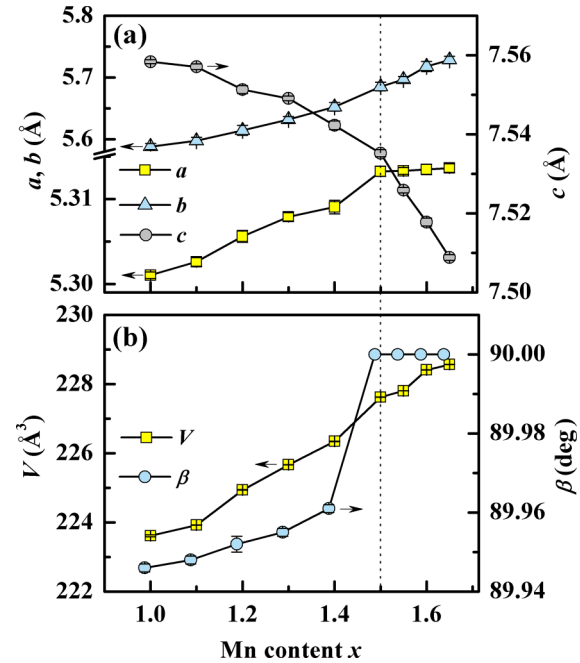

FIG. 2. (a) and (b) Mn content x dependence of the lattice parameters.

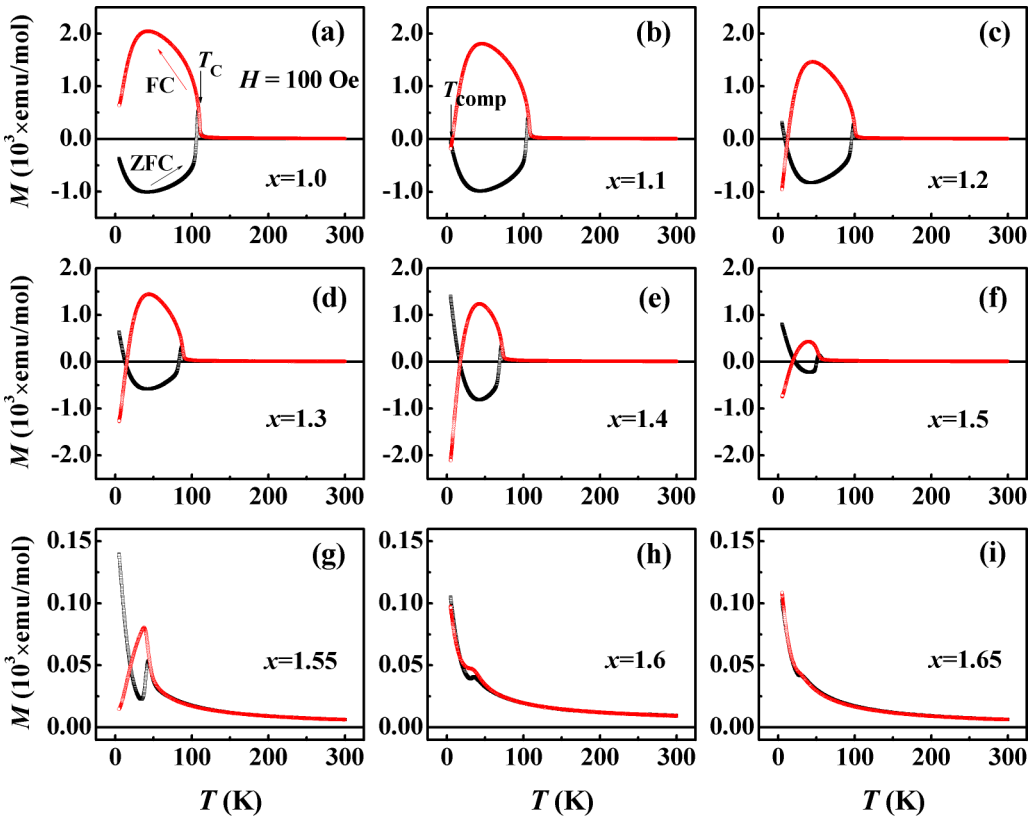

FIG. 3. (a)−(i) Temperature-dependent zero-field-cooled (ZFC) and field-cooled (FC) magnetization under H= 100 Oe for the samples of $Gd_2Co_{2-x}Mn_xO_6$ ($1.0 \leqslant x \leqslant 1.65$).

a monoclinic structure with $\beta \neq 90^\circ$ at $1.0 \leqslant x \leqslant 1.4$ and an orthorhombic structure with $\beta = 90^\circ$ at $1.5 \leqslant x \leqslant 1.65$. The lattice parameters of $Gd_2Co_{2-x}Mn_xO_6$ in this paper are close to the previously reported values [20,21].

The magnetic properties of $Gd_2Co_{2-x}Mn_xO_6$ were measured upon heating from 5 to 300 K under a stable magnetic field H= 100 Oe after a zero-field-cooling (ZFC) process and then field cooling (FC) from 300 to 5 K under the same H. As shown in Fig. 3(a), both the ZFC and FC magnetization for the parent compound at $x = 1.0$ increases sharply when the measurement temperature is close to $T_C = 111$ K, suggesting rapid arrangement of FM domains along the direction of H. The FM order can be identified as the sharp anomaly in the T derivative M, which is dominated by the superexchange interactions between Co^{2+} and Mn^{4+} according to the Goodenough-Kanamori rule [32]. The curves of the two modes exhibit distinct bifurcation and irreversibility, implying strong magnetocrystalline anisotropy. The decrease in FC magnetization <43 K is ascribed to the complex magnetic interactions between Gd^{3+} and Co^{2+}/Mn^{4+} sublattices due to the short-range AFM order of Gd^{3+} [21]. The negative magnitude of M in the ZFC process is attributed to a typical remanent H that persists negatively upon cooling [10,12,13,19]. With the increase in the relative proportion of Mn, the FM ordering temperature is progressively decreased from 111 K at $x = 1.0$ to 34 K at $x = 1.65$. As shown in Fig. 3(b), it is important to note that the $M(T)$ curves display a crossover of the M= 0 axis at compensation temperature $T_{comp} = 7$ K, and the FC magnetization M_{FC} even becomes negative though the applied H is positive (+100 Oe). This is the so-called NM, and a similar phenomenon has also been observed in undoped spinels [33,34] and distorted honeycomb ceramics [35,36] as well as several complex perovskite compounds [37,38]. The NM associated with $M_{FC} < 0$ is rare in polycrystalline systems owing to the tendency of the spins to align with the applied H. In this paper, as shown in Figs. 3(b)–3(i), the NM starts from $x = 1.1$ and continues until $x = 1.5$. It disappears completely at $x = 1.55$, but the FC curve still shows a downward trend under low T. The phase dominated at low T for x>1.55 is obviously different from the low relative proportion of Mn for $x = 1.0-1.5$. The evolution of the magnetic phase with Mn content and temperature will be discussed later.

To obtain in-depth information, two parameters characterizing the NM, i.e., M_{FC} at 5 K and compensation temperature T_{comp} as a function of Mn content x are depicted in Fig. 4. The level of the NM reaches the highest at $x = 1.4$ with $M_{FC} = -2105$ emu/mol, and it reduces monotonically with the increase/decrease of Mn relative proportion. The non-monotonic NM with doping amount has also been reported in chromium-based spinel systems [4,5]. The absolute values of M_{FC} for the samples associated with the NM, except for the sample at $x = 1.1$ with $M_{FC} = -181$ emu/mol, are even larger than the samples connected with positive M_{FC} for $x = 1.0$, $1.55-1.65$ with $M_{FC} = 637$, $15-108$ emu/mol, respectively. The other parameter T_{comp} is monotonically increased from 7 K at $x = 1.1$ to 19 K at $x = 1.5$. The lack of T_{comp} for $x = 1.0$, $1.55-1.65$ is owing to the absence or disappearance of NM. The observation of NM indicates that

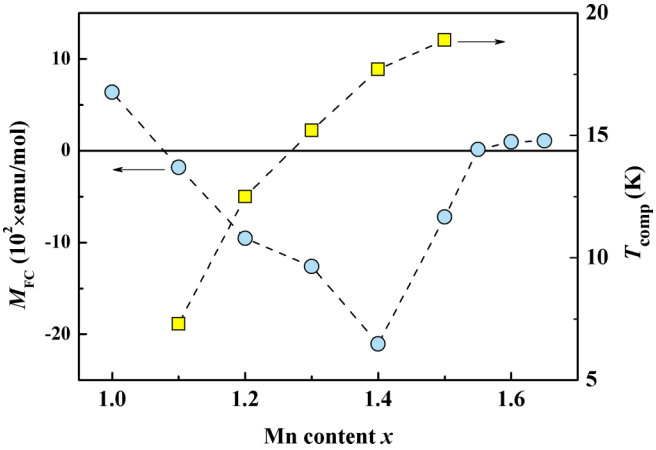

FIG. 4. Mn content x dependence of the field-cooled (FC) magnetization at 5 K (M_{FC}) and compensation temperature (T_{comp}).

inverse magnetic moments are dominant and net magnetic moments are antiparallel to the applied magnetic field under low temperature.

For more details about the NM, the samples at $x = 1.2$ and 1.4 were measured as representative in different protocols of the FC mode. As shown in Figs. 5(a) and 5(b), the experimental fact shows that the FC curves under +500 and −500 Oe magnetic fields are almost axisymmetric with respect to the temperature axis. The NM characterized by $M(T_{comp}) = 0$ in the FC curves occurs almost simultaneously when the magnitudes of applied magnetic fields are the same but their directions are opposite, indicating that the effect in

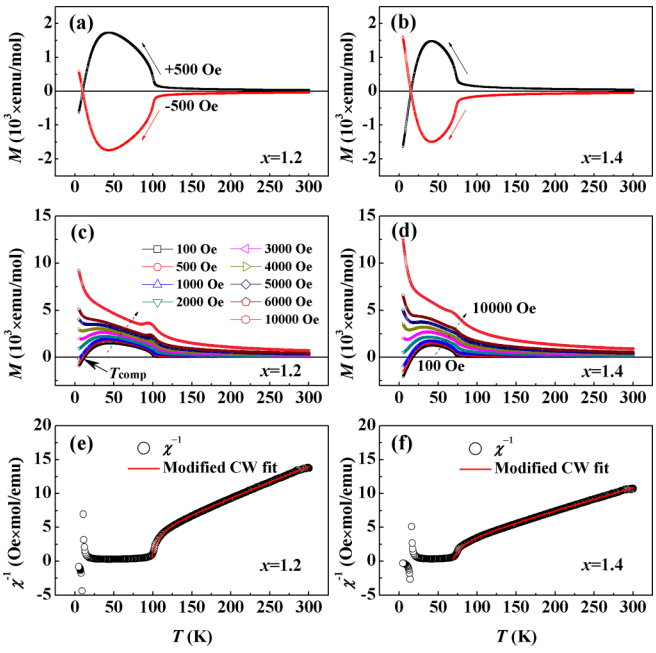

FIG. 5. Field-cooled (FC) curves measured under ±500 Oe for the samples at (a) $x = 1.2$ and (b) $x = 1.4$. FC curves measured under various H ranging from 100 to 10 000 Oe for (c) $x = 1.2$ and (d) $x = 1.4$. Modified Curie-Weiss (CW) fit for (c) $x = 1.2$ and (d) $x = 1.4$.

$Gd_2Co_{2-x}Mn_xO_6$ is intrinsic. The mirrorlike FC behavior is also considered as one of the symbols of the NM. To further investigate the response of magnetization to the temperature, the FC magnetization was recorded under various magnetic fields ranging from 100 to 10 000 Oe. As depicted in Figs. 5(c) and 5(d), the magnetization is negative below T_{comp} as the magnetic field $H \leqslant 1000$ Oe, while it becomes positive in the whole measuring temperature range under higher magnetic fields. It is evident that the magnetization state can be tuned effectively by adjusting the magnetic field strength. In addition, the results show a sharp increase in magnetization characterized by the upturn in $M(T)$ curves associated with large magnetic moments of Gd^{3+} under $H \geqslant 3000$ Oe. In other words, the spin moments of Gd^{3+} (the orbital angular momentum L is zero) align along the direction of the applied H above a threshold value. Therefore, the inverse magnetic moments in $Gd_2Co_{2-x}Mn_xO_6$ are mainly contributed by Gd^{3+} spin moments, which are antiparallel to the Co/Mn sublattices, as well as the applied H.

The inverse magnetic susceptibility χ^{-1} vs temperature T is shown in Figs. 5(e) and 5(f). The linear $\chi^{-1}(T)$ curve at high T represents the paramagnetic (PM) state, while the curve deviates from the linear behavior with a downward curvature near T_C. It implies that both Gd and Co/Mn sublattices contribute to the total susceptibility. For the sake of comparison, the $M(T)$ and $\chi^{-1}(T)$ curves of Y_2CoMnO_6 were also investigated in Fig. S2 in the Supplemental Material [31]. The linear fit of the $\chi^{-1}(T)$ curve at high T for nonmagnetic rare-earth Y-, La-, or Lu-based DPs in this paper or the literature [26,39] confirms the contribution of Gd ions to the total susceptibility. Therefore, the $\chi^{-1}(T)$ curves are fitted by a modified Curie-Weiss (CW) law with the expression $\chi(T) = \chi_{TM} + \chi_{RE} = \frac{C_{TM}}{T-\Theta_{TM}} + \frac{C_{RE}}{T-\Theta_{RE}}$, where C_{TM} and C_{RE} are the Curie constants, θ_{TM} and θ_{RE} are the CW temperatures. The subscripts TM and RE denote transition metal ions and rare-earth ions, respectively. The nonlinear fits with the equation are shown as solid lines in Figs. 5(e) and 5(f). This type of fit is often utilized for DPs with both rare-earth and transition metal ions [40,41]. The experimental data can be well fitted over a wide temperature range. The parameters generated by the fitting show that θ_{TM} values for the samples at $x = 1.2$ and 1.4 are 99.2 and 71.8 K, respectively, which are close to their T_C. The positive θ_{TM} suggests that the multiple interactions between transition metal ions are mainly FM. The effective PM magnetic moments μ_{eff} can be calculated by the formula $\mu_{eff} = \frac{1}{\mu_B}(\frac{3k_BC}{N_A})^{1/2}$, where μ_B is the Bohr magneton, k_B is the Boltzmann constant, and N_A is the Avogadro constant. The calculated μ_{eff}(TM) values for the sample at $x = 1.2$ and 1.4 are 4.0 μ_B and 4.4 μ_B, respectively. Both the experimental values are smaller than that of the theoretical value. This is presumably owing to the low spin state of TM ions as reported in previous Co/Mn-based DPs [41,42]. Additionally, the calculated μ_{eff}(RE) values for the samples at $x = 1.2$ and 1.4 are 12.3 μ_B and 13.1 μ_B, respectively, which are close to the theoretical value of Gd^{3+}.

Based on the above experimental results, the temperature (T) and magnetic field (H) not only induce the magnetic compensation effect characterized by $M(T) = 0$ at $T = T_{comp}$ under a moderate H but also affect the magnetization state around

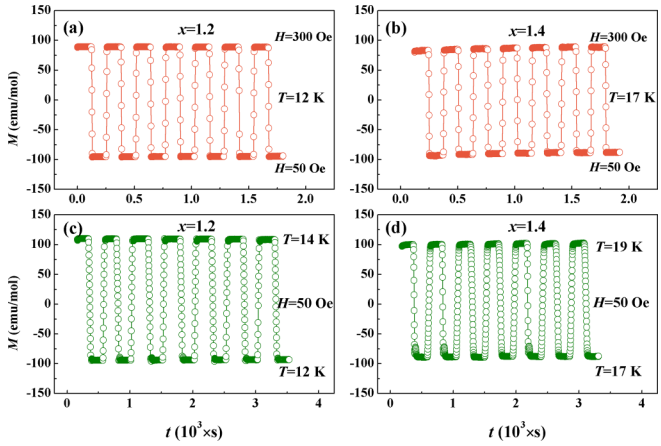

FIG. 6. Magnetic-field-assisted switching effect from 50 to 300 Oe (a) at 12 K for $x = 1.2$ and (b) at 14 K for $x = 1.4$. Thermal-assisted switching effect under 50 Oe (c) from 12 to 14 K for $x = 1.2$ and (d) from 17 to 19 K for $x = 1.4$.

T_{comp}. Therefore, this intriguing effect has aroused our great interest to manipulate the magnetization states by adjusting the applied T and H. To begin with, H-assisted switching effects were measured by the following steps. The sample is subjected to field cooling to 12 K (17 K) at $x = 1.2$ ($x = 1.4$) and the magnetization is recorded for half a period under 300 Oe. The applied H is then reduced to 50 Oe, and the measurement continues for the remaining half cycle. After such a measurement lasts for some cycles, the obtained results are shown in Figs. 6(a) and 6(b), respectively. It is important to realize that the magnetization state is determined by the magnitude of the applied H, and the manipulation of H on magnetization state is freely almost without decay. Furthermore, T-assisted switching effects for the samples at $x = 1.2$ and 1.4 are shown in Figs. 6(c) and 6(d), respectively. The sample is firstly cooled to 14 K (19 K) at $x = 1.2$ ($x = 1.4$) under a stable H of 50 Oe, and the magnetization is recorded for half a period. The applied T is then decreased to 12 K (17 K) at $x = 1.2$ ($x = 1.4$), and the measurement continues for the remaining half cycle. Such measurements last for several cycles, and it is found that manipulation of T on magnetization state is also free. Therefore, the results presented in Fig. 6 indicate that the magnetization state can be switched from positive to negative and vice versa by adjusting the applied T or H. The H- or T-assisted switching effect exhibits promising applications in spintronic devices.

Figures 7(a) and 7(b) display the isothermal $M(H)$ hysteresis loops at 5 K measured under the FC condition ($H_{cool} = \pm 1$ kOe) for the samples at $x = 1.2$ and 1.4, respectively. The $M(H)$ shows small coercivity (H_C), and the exchange bias (EB) effect is observed as characterized by the horizontal shift of the loop. It is worth noting that the shift is in the same direction of H_{cool}, i.e., the shift is along $+H$ under $+H_{cool}$, while it is along $-H$ under $-H_{cool}$. The shift is contrary to the conventional EB effect [43]. The presence of inverse EB suggests that NM can also be realized by the suitable application of H. The H_C value increases with an increase in temperature, as shown in Figs. 7(c) and 7(d). However, the shift of $M(H)$ loops is along $-H$ under $+H_{cool}$, indicating the EB effect

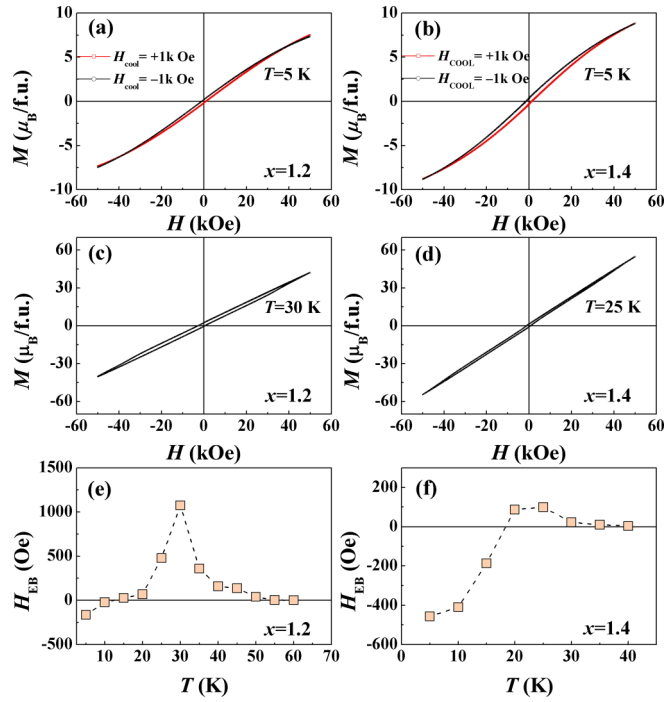

FIG. 7. $M(H)$ hysteresis loops measured under $H_{cool} = \pm 1000$ Oe at 5 K for the samples at (a) $x = 1.2$ and (b) $x = 1.4$. $M(H)$ hysteresis loops measured at 30 and 25 K for the samples at (c) $x = 1.2$ and (d) $x = 1.4$. H_{EB} as a function of temperature for the samples at (e) $x = 1.2$ and (f) $x = 1.4$.

is reversed under higher temperatures. The EB is defined on the basis of the exchange field $H_{EB} = (|H_{C1}| - |H_{C2}|)/2$ [13,44], where H_{C1} and H_{C2} are the coercive fields where the $M(H)$ loops intersect the H axis on the left and right sides, respectively. The temperature dependence of H_{EB} for the samples at $x = 1.2$ and 1.4 is displayed in Figs. 7(e) and 7(f), respectively. The H_{EB} value is somewhat large despite the fact that H_C is quite small, which is like the previous reported Gd-based DPs [12,13,45]. For instance, in the sample at $x = 1.2$, the value of H_{EB} shows a minimum of -163 Oe at 5 K and a maximum of 1075 Oe at 30 K. In the sample at $x = 1.4$, H_{EB} shows a minimum of -457 Oe at 5 K and a maximum of 100 Oe at 25 K. Apparently, an inverse EB effect with negative H_{EB} is obtained at low temperatures, while the conventional EB with positive H_{EB} is observed at higher temperatures. The temperature of sign change of H_{EB} is very close to the compensation temperature T_{comp} of the samples at $x = 1.2$ and 1.4 (see Fig. 4). Additionally, the isothermal FC $M(H)$ curves were measured under various cooling fields, and the results are depicted in Figs. S3 and S4 in the Supplemental Material [31]. The $M(H)$ loops for the sample at $x = 1.2$ are relatively narrow. The finite EB effect can be seen from the $M(H)$ curves, which exhibit a characteristic shift along the H axis. The EB field H_{EB} and remanence asymmetry M_{EB} as a function of cooling field H_{cool} for the samples at $x = 1.2$ and 1.4 are shown in Fig. S5 in the Supplemental Material [31]. Here, M_{EB} is defined as $M_{EB} = (|M_1| - |M_2|)/2$, where M_1 and M_2 are the remnant magnetization at the descending and ascending branches of the $M(H)$ loop, respectively. It can be noticed that both the magnitudes of H_{EB} and M_{EB} rise sharply

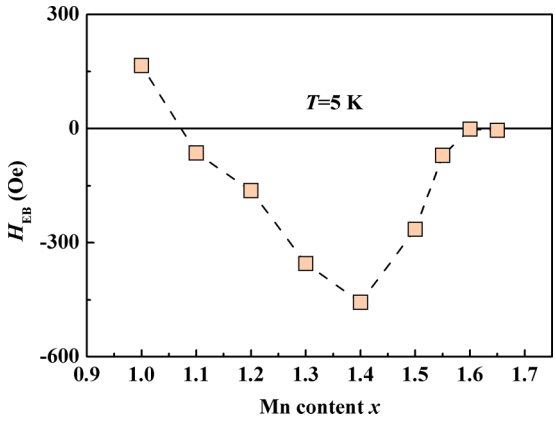

FIG. 8. Mn content x dependence of exchange bias field H_{EB}.

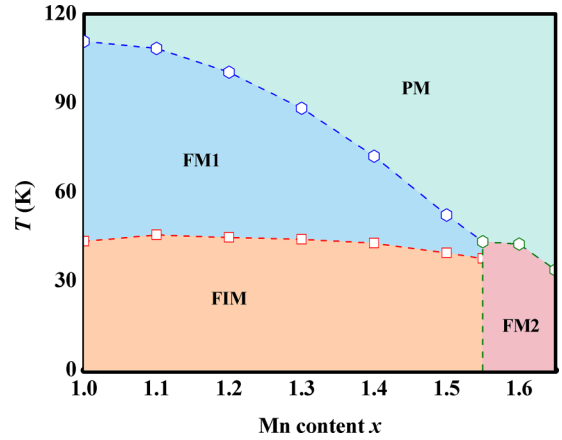

FIG. 9. Mn content x and temperature (x-T) phase diagram of $Gd_2Co_{2-x}Mn_xO_6$. PM and FIM represent paramagnetic and ferrimagnetic phases, respectively. FM1 and FM2 represent the ferromagnetic phases at different stages.

at low H_{cool}, suggesting an increasing number of pinned spins. Their magnitudes decrease with further enhancing H_{cool} up to 30 kOe, which is in contrast to the behavior of the conventional EB effect with a sign reversal of the EB effect under high H_{cool} [46,47]. In addition to rightward horizontal shifts from the origin, the hysteresis loops display downward vertical shifts, which suggest that the magnetic moment direction is opposite the applied H_{cool}.

Additionally, the FC $M(H)$ hysteresis loops for all $Gd_2Co_{2-x}Mn_xO_6$ ($1.0 \leqslant x \leqslant 1.65$) samples were measured after cooling the samples from 150 K (well above T_C) to 5 K, and H_{EB} was evaluated based on the above equation. The H_{EB} as a function of Mn content x is plotted in Fig. 8. It is evident that the samples with NM or a downward trend of the FC curve (see Fig. 3) display an inverse EB, except for the sample at $x = 1.0$. The parent sample Gd_2CoMnO_6 exhibits a conventional EB that originates from the unidirectional anisotropy induced at the AFM/FM interface [45]. The absence of EB in the samples at $x > 1.55$ is presumably associated with the excess AFM phase which is comparable with the dominant FM phase and would not act as efficient pinning centers [19]. Furthermore, we notice that the curve shows a valley at $x = 1.4$, which is consistent with the level of NM as characterized by M_{FC} at 5 K (see Fig. 4) as well as the structural phase transition (see Fig. 2). This indicates that the observed magnetic anomalies including NM and the inverse EB effect may have the same physical origin.

IV. DISCUSSION

Finally, we discuss the Mn substitution on NM and the EB effect of $Gd_2Co_{2-x}Mn_xO_6$ compounds. Based on the above magnetic measurements, the Mn content x and temperature (x-T) phase diagram of $Gd_2Co_{2-x}Mn_xO_6$ is constructed in Fig. 9. The x-T phase diagram shows obvious phase boundaries, and one sample undergoes three distinct major phases, labeled as high-T PM, low-T FIM, or FM2 phases, as well as the intermediate-T FM1 phase between them. From the legible x-T phase diagram, one can infer that the relative proportion of Mn and temperature has significant effects on the magnetic structure of the $Gd_2Co_{2-x}Mn_xO_6$ system. Here, the FM1 phase mainly results from Co^{2+}–O^{2-}–Mn^{4+} superexchange interactions, as indicated in most Co/Mn-based DPs [18,19,21]. The excessive ratio of Mn induces two charge states of Mn ions (Mn^{3+} and Mn^{4+}) due to charge compensation. The contribution of Co^{3+} is neglected because of its low spin state (with zero magnetic moment) [41,42,48], which has been suggested by the fact that the experimental value of μ_{eff} is smaller than the theoretical value. The absence of NM in Gd_2CoMnO_6 suggests that the moment of Gd^{3+} is not enough to overcome the Co^{2+} and Mn^{4+} resultant moment. Therefore, the NM characterized by $M_{FC} < 0$ in the samples from $x = 1.1$ to 1.5 suggests that the Mn^{3+} moment tends to align in the same direction as the Gd^{3+} sublattice. The Gd^{3+} ordering temperature is identified by the decrease in $M_{FC} < 43$ K, and it is almost independent of the Mn proportion [see Figs. 3(a)–3(i)]. The NM originating from negative exchange coupling among different sublattices has also been investigated in FIM manganite $GdBaMn_2O_5$ [49]. The observation of NM or a downward trend of the FC curve suggests that the FIM structure composed of Gd^{3+} and Co/Mn sublattices is formed; the sublattices have different temperature dependences according to the Néel theory [50]. In other words, the existence of NM indicates that inverse magnetic moments play a dominant role at low T, and the net magnetic moments are antiparallel to the applied H. However, such a FIM structure changes with the further increase in Mn proportion. The FM2 phase dominated by positive exchange coupling between Gd^{3+} and Co/Mn sublattices is formed which is characterized by the rapid increase in $M(T)$ curves below the Gd^{3+} ordering temperature [see Figs. 3(h) and 3(i)].

As is well known, the classical model of the conventional EB effect originates from the interfacial coupling between the AFM phase with strong anisotropy and the FM phase with weak anisotropy. The unidirectional anisotropy developed at the interface and the pinning force provided by the AFM phase result in the horizontal shift of $M(H)$ loops along the opposite direction of H. In this paper, the sample at $x = 1.0$ conforms to this physical model. With an increase in the Mn relative proportion, multiple magnetic interactions are aroused by antisite disorder due to the excessive ratio of Mn ions that give rise to inhomogeneous magnetic phases. The increase in

relative proportion of Mn not only instigates antisite disorder, evoking like $Mn^{4+}-O^{2-}-Mn^{4+}$ and $Co^{2+}-O^{2-}-Co^{2+}$ AFM interactions, but also possibly induces Mn-rich clusters owing to the large amount of Mn [19]. The magnetization contributed by the AFM phase is finite, but the AFM regions are crucial in separating the abundant FM clusters [10,13]. In addition, the mixed valence of Co and Mn may also produce additional exchange interactions such as $Mn^{3+}-O^{2-}-Mn^{3+}$, $Mn^{3+}-O^{2-}-Mn^{4+}$, and $Co^{2+}-O^{2-}-Mn^{3+}$. Moreover, as shown in Figs. 7(e) and 7(f), H_{EB} displays a very similar change with reversal of sign across T_{comp}, implying evidence of the same underlying mechanism for both the inverse EB and NM.

It is necessary to point out that the inverse EB is known to occur in classic AFM/FM interface systems when the cooling field is large enough to overcome the AFM interfacial coupling ($J < 0$) [46,47]. In other words, the conventional EB can be observed under low H_{cool} due to the opposite direction of AFM spins at the interface and applied magnetic field, while the inverse EB appears under high H_{cool} since the AFM spins are rotated along the applied field. The sharp increase of the magnitudes of H_{EB} and M_{EB} at low H_{cool} is like the AFM/FM phase-separated systems [43,44], indicating that the anisotropy energy barrier of the studied system is small, which can be overcome only by small H_{cool}. However, such a scenario is ruled out in this paper since there is no sign reversal of the EB field with the variation of H_{cool} (see Fig. S5 in the Supplemental Material [31]). The EB remains inverse up to $H_{cool} = 30$ kOe, and both the magnitudes of H_{EB} and M_{EB} decrease with further increasing H_{cool}. Therefore, the AFM/FM phase-separated model is not suitable for the system studied in this paper.

The inverse EB has been reported in several magnetic systems simultaneously presenting NM phenomenon, and several origins were proposed. For instance, the thermally induced NM and inverse EB have been recently investigated in DPs Er_2CoMnO_6 [12] and Gd_2CoRuO_6 [13], where the EB in the former is attributed to the negative exchange interaction at the interface of ordered and antisite disorder FIM phases, while in the latter, it is ascribed to the mixed interfacial coupling between adjacent magnetic nanoclusters. The EB in the two compounds is significantly different from the research objects in this paper, as neither of them show EB change with reversal of sign across T_{comp}. On the other hand, the spinel compounds $Co(Cr_{0.95}Fe_{0.05})_2O_4$ [7] and $Co(Cr_{0.7}Mn_{0.3})_2O_4$ [51] exhibit distinctive EB behavior, where H_{EB} approaches zero when the measurement temperature is far from T_{comp}, while it rises and diverges when the temperature is close to T_{comp}. It can be explained well by the Webb model [52], where H_{EB} is varied inversely with the net magnetic moment, and its sign depends on the direction of the net magnetic moment in relation to the applied field. However, such an unusual H_{EB} variation is also different from the situation in this paper. We also notice that the sign change of H_{EB} across T_{comp} has been found recently in perovskite $YbCrO_3$ [53] and DP Sr_2YbRuO_6 [54], which is in contrast to the above spinel compounds. Below T_{comp}, a relatively lower magnetic field is required to change the magnetization from positive to negative during the descending branch of the $M(H)$ loop from $+H_{max}$ ($= 50$ kOe) to $-H_{max}$ ($= -50$ kOe). Because the NM state is favored at $T < T_{comp}$, it thus results in a low left coercive field, while on the ascending branch from $-H_{max}$ to $+H_{max}$, a higher magnetic field is necessary to flip the NM state to positive since the positive state is energetically unfavorable at $T < T_{comp}$. Therefore, a higher right coercive field is obtained. Once the above model is accepted, it is reasonable to explain the inverse EB effect observed at $T < T_{comp}$. Below the FIM compensation point, the NM phenomenon suggests the net weak FM moments align opposite to the applied $+H_{cool}$. Therefore, the negative remanence is induced during the FC process, and it served as the initial state of the hysteresis loop, though the applied field is set to zero before the $M(H)$ measurement. Such a scenario is consistent with the available literature concerning NM, which is assigned to the NM state below the FIM compensation point, and the polarity of the EB effect is determined by the initial state [55,56]. Although we have given a reasonable scenario for the experimental observation, a more comprehensive model is required to be proposed to specify the magnetic structures in the future.

V. CONCLUSIONS

To conclude, the polycrystalline $Gd_2Co_{2-x}Mn_xO_6$ ($1.0 \leqslant x \leqslant 1.65$) perovskites were synthesized, and their magnetic properties were experimentally investigated. To begin with, the FM transition temperature is progressively decreased from 111 K at $x = 1.0$ to 34 K at $x = 1.65$. Intrinsic effects including the compensation effect depicted by $M(T_{comp}) = 0$ and NM characterized by $M_{FC} < 0$ under a moderate positive magnetic field are observed in the samples from $x = 1.1$ to 1.5. The level of NM reaches the highest at $x = 1.4$ with $M_{FC} = -2105$ emu/mol, and it reduces with the increase/decrease of the Mn relative proportion. The compensation temperature T_{comp} is monotonically increased from 7 K at $x = 1.1$ to 19 K at $x = 1.5$. Furthermore, the magnetization state of the sample with NM can be switched from positive to negative and vice versa by adjusting the applied T or H. By manipulating the magnetization state, the H- or T-assisted switching effect exhibits promising applications in spintronic devices. In addition, there is a sign reversal of the EB field vs temperature, and an inverse EB effect is observed below T_{comp}, which is characterized by the horizontal shift of the $M(H)$ loops toward H_{cool}. The absence of a sign change of the EB field vs the cooling field contrasts with the conventional AFM/FM interface systems. The observed NM is explained by considering a FIM structure to be formed which has different temperature dependence of sublattice magnetic moments. The inverse nature of EB has the same physical origin as NM, which is attributed to the opposite alignment of the net FM moments to the applied cooling field below the FIM compensation point.

ACKNOWLEDGMENTS

This paper was supported by Key Research Projects of Henan Provincial Department of Education (Grant No. 21A140024), National Natural Science Foundation of China (Grant No. 12074328), Natural Science Foundation of Henan Province (Grants No. 232300421353 and No. 232300420121), and Nanhu Scholars Program for Young Scholars of XYNU. This paper was also supported by the Analysis & Testing Center of XYNU.

[1] A. Kumar and S. M. Yusuf, The phenomenon of negative magnetization and its implications, Phys. Rep. **556**, 1 (2015).

[2] C. L. Li, S. Huang, X. X. Li, C. M. Zhu, G. Zerihun, C. Y. Yin, C. L. Lu, and S. L. Yuan, Negative magnetization induced by Mn doping in $YCrO_3$, J. Magn. Magn. Mater. **432**, 77 (2017).

[3] C. L. Li, S. S. Zheng, G. O. Barasa, Y. F. Zhao, L. Wang, C. L. Wang, Y. Lu, Y. Qiu, J. B. Cheng, and Y. S. Luo, A comparative study on magnetic behaviors and magnetocaloric effect in heavy rare-earth antiferromagnetic orthoferrites $RFeO_3$ (R = Dy, Ho and Er), Ceram. Int. **47**, 35160 (2021).

[4] C. L. Li, C. L. Wang, Q. K. Lei, G. O. Barasa, Q. S. Fu, and Y. Qiu, Effect of Fe substitution on structure and exchange interactions within and between the sublattices of frustrated $CoCr_2O_4$, Phys. Chem. Chem. Phys. **22**, 28222 (2020).

[5] B. Meng, Q. S. Fu, X. H. Chen, G. S. Gong, C. Chakrabarti, Y. Q. Wang, and S. L. Yuan, Effect of Al substitution on the magnetization reversal and complex magnetic properties of $NiCr_2O_4$ ceramics, Phys. Chem. Chem. Phys. **24**, 4925 (2022).

[6] Y. Qiu, S. S. Zheng, C. L. Li, G. O. Barasa, M. L. Chen, L. Wang, Y. F. Zhao, Y. Lu, and Y. S. Luo, Size-dependent compensation effect and negative magnetization in $Co(Cr_{0.9}Fe_{0.1})_2O_4$ annealed at different temperatures, J. Alloy. Compd. **901**, 163692 (2022).

[7] R. Padam, S. Pandya, S. Ravi, A. K. Nigam, S. Ramakrishnan, A. K. Grover, and D. Pal, Magnetic compensation effect and phase reversal of exchange bias field across compensation temperature in multiferroic $Co(Cr_{0.95}Fe_{0.05})_2O_4$, Appl. Phys. Lett. **102**, 112412 (2013).

[8] C. L. Li, G. O. Barasa, Y. Qiu, and S. L. Yuan, Magnetocaloric effect and sign reversal of magnetic entropy change across the spin reorientation temperature in $R_3Fe_5O_{12}$ (R = Gd, Dy), J. Alloy. Compd. **820**, 153138 (2020).

[9] M. Ghanathe, A. Kumar, I. da Silva, and S. M. Yusuf, Magnetic ordering of Ho and its role in the magnetization reversal and coercivity double peaks in the $Ho_3Fe_5O_{12}$ garnet, J. Magn. Magn. Mater. **523**, 167632 (2021).

[10] H. G. Zhang, L. Xie, X. C. Liu, M. X. Xiong, L. L. Cao, and Y. T. Li, The reversal of the spontaneous exchange bias effect and zero-field-cooling magnetization in $La_{1.5}Sr_{0.5}Co_{1-x}Fe_xMnO_6$: The effect of Fe doping, Phys. Chem. Chem. Phys. **19**, 25186 (2017).

[11] L. Xie and H. G. Zhang, Zero-field cooled exchange bias and magnetization reversal in $La_{1.5}Sr_{0.5}Co_{0.4}Fe_{0.6}MnO_6$, Curr. Appl. Phys. **18**, 261 (2018).

[12] A. Banerjee, J. Sannigrahi, S. Giri, and S. Majumdar, Magnetization reversal and inverse exchange bias phenomenon in the ferrimagnetic polycrystalline compound Er_2CoMnO_6, Phys. Rev. B **98**, 104414 (2018).

[13] M. Das, P. Dutta, S. Giri, S. Majumdar, A. Bandyopadhyay, A. K. Yadav, S. N. Jha, D. Bhattacharyya, G. Das, and V. Rajaji, Cationic disorder: A pathway for demonstrating inverse exchange bias in Gd_2CoRuO_6, Phys. Rev. B **101**, 064419 (2020).

[14] A. Marsh and C. C. Clark, Metamagnetism in the perovskite compound Gd_2CoMnO_6, Philos. Mag. **19**, 449 (1969).

[15] J. Krishna Murthy, K. Devi Chandrasekhar, S. Mahana, D. Topwal, and A. Venimadhav, Giant magnetocaloric effect in Gd_2NiMnO_6 and Gd_2CoMnO_6 ferromagnetic insulators, J. Phys. D: Appl. Phys. **48**, 355001 (2015).

[16] S. S. Zheng, C. L. Li, C. X. Bai, K. X. Zhou, P. Wang, Y. Lu, Y. Qiu, and Y. S. Luo, Magnetic properties and enhanced cryogenic magnetocaloric effect in Ti-substituted Gd_2CoMnO_6 double perovskites, J. Magn. Magn. Mater. **564**, 170162 (2022).

[17] C. L. Li, S. S. Zheng, Y. Qiu, Q. K. Lei, C. L. Wang, Y. Lu, Y. Yang, H. L. Yan, and Y. S. Luo, Effect of Ti substitution on structural, magnetic and magnetocaloric properties in double perovskites $Gd_2NiMn_{1-x}Ti_xO_6$ ($0 \leqslant x \leqslant 1$), Ceram. Int. **49**, 6891 (2023).

[18] J. K. Murthy, K. D. Chandrasekhar, H. C. Wu, H. D. Yang, J. Y. Lin, and A. Venimadhav, Antisite disorder driven spontaneous exchange bias effect in $La_{2-x}Sr_xCoMnO_6$ ($0 \leqslant x \leqslant 1$), J. Phys.: Condens. Matter. **28**, 086003 (2016).

[19] S. H. Oh, J. Y. Moon, D. G. Oh, Y. J. Choi, and N. Lee, Enhanced exchange bias effect by modulating relative ratio of magnetic ions in $Y_2Co_{2-x}Mn_xO_6$ ($x = 1.0-1.9$), Phys. Status Solidi RRL **13**, 1900008 (2019).

[20] M. K. Kim, J. Y. Moon, H. Y. Choi, S. H. Oh, N. Lee, and Y. J. Choi, Investigation of the magnetic properties in double perovskite R_2CoMnO_6 single crystals (R = rare earth: La to Lu), J. Phys.: Condens. Matter. **27**, 426002 (2015).

[21] M. Das, P. Sarkar, and P. Mandal, Non-Griffiths-like cluster formation in the double-perovskite Gd_2CoMnO_6: Evidence from critical behavior, Phys. Rev. B **101**, 144433 (2020).

[22] H. Y. Zhou and X. M. Chen, Structural distortions, orbital ordering and physical properties of double perovskite R_2CoMnO_6 calculated by first-principles, J. Phys.: Condens. Matter. **29**, 145701 (2017).

[23] H. S. Nair, R. Pradheesh, Y. Xiao, D. Cherian, S. Elizabeth, T. Hansen, T. Chatterji, and T. Brückel, Magnetization-steps in Y_2CoMnO_6 double perovskite: The role of antisite disorder, J. Appl. Phys. **116**, 123907 (2014).

[24] A. K. Singh, S. Chauhan, S. K. Srivastava, and R. Chandra, Influence of antisite disorders on the magnetic properties of double perovskite Nd_2NiMnO_6, Solid State Commun. **242**, 74 (2016).

[25] R. I. Dass and J. B. Goodenough, Multiple magnetic phases of $La_2CoMnO_{6-\delta}$ ($0 \leqslant \delta \leqslant 0.05$), Phys. Rev. B **67**, 014401 (2003).

[26] S. Yáñez-Vilar, E. D. Mun, V. S. Zapf, B. G. Ueland, J. S. Gardner, J. D. Thompson, J. Singleton, M. Sánchez-Andújar, J. Mira, N. Biskup *et al.*, Multiferroic behavior in the double-perovskite Lu_2MnCoO_6, Phys. Rev. B **84**, 134427 (2011).

[27] A. Harbi, Y. Le Godec, H. Moutaabbid, S. Benmokhtar, and M. Moutaabbid, Tailoring the Griffiths-like cluster formation in the insulator ferromagnet spin-glass $Gd_2Ni_xCo_{1-x}MnO_6$ double perovskite, Phys. Rev. B **104**, 054404 (2021).

[28] C. H. Prashanth, I. R. Reddy, K. Tarafder, D. C. Kakarla, H. D. Yang, V. Adyam, and K. Jyothinagaram, Magnetic complexity, magnetodielectric effect and DFT calculations on correlation driven Gd_2CoMnO_6 insulator, J. Magn. Magn. Mater. **563**, 169880 (2022).

[29] X. L. Wang, J. Horvat, H. K. Liu, A. H. Li, and S. X. Dou, Spin glass state in Gd_2CoMnO_6 perovskite manganite, Solid State Commun. **118**, 27 (2001).

[30] A. R. Denton and N. W. Ashcroft, Vegard's law, Phys. Rev. A. **43**, 3161 (1991).

[31] See Supplemental Material at http://link.aps.org/supplemental/10.1103/PhysRevB.107.214445 for the x-ray photoelectron spectroscopy (XPS) data for $Gd_2Co_{2-x}Mn_xO_6$ ($x = 1.0, 1.2, 1.4$, and 1.6), zero-field-cooled (ZFC) and field-cooled (FC) curves for Y_2CoMnO_6, $M(H)$ curves for the samples at $x = 1.2$ and 1.4 after being cooled under 100, 300,

500, and 30000 Oe fields, and EB field H_{EB} and remanence asymmetry M_{EB} for the samples at $x = 1.2$ and 1.4.

[32] J. B. Goodenough, A. Wold, R. J. Arnott, and N. Menyuk, Relationship between crystal symmetry and magnetic properties of ionic compounds containing Mn^{3+}, Phys. Rev. **124**, 373 (1961).

[33] S. Nayak, S. Thota, D. C. Joshi, M. Krautz, A. Waske, A. Behler, J. Eckert, T. Sarkar, M. S. Andersson, R. Mathieu, V. Narang, and M. S. Seehra, Magnetic compensation, field-dependent magnetization reversal, and complex magnetic ordering in Co_2TiO_4, Phys. Rev. B **92**, 214434 (2015).

[34] Q. S. Fu, C. L. Li, B. Meng, C. Chakrabarti, R. Zhang, X. H. Chen, Y. H. Li, and S. L. Yuan, Effect of annealing temperature on structural and magnetic properties of Co_2TiO_4 ceramics prepared by sol-gel method, Ceram. Int. **45**, 6906 (2019).

[35] B. Meng, X. T. Ji, X. H. Chen, Q. S. Fu, C. L. Li, C. Chakrabarti, Y. Qiu, and S. L. Yuan, Negative magnetization effect in distorted honeycomb $Ni_4Nb_2O_9$ ceramics, J. Low Temp. Phys. **207**, 115 (2022).

[36] S. Thota, M. S. Seehra, M. R. Chowdhury, H. Singh, S. Ghosh, S. K. Jena, P. Pramanik, T. Sarkar, R. S. Rawat, R. Medwal *et al.*, Unraveling the nature of ferrimagnetism and associated exchange interactions in distorted honeycomb $Ni_4Nb_2O_9$, Phys. Rev. B **106**, 134418 (2022).

[37] K. Vijayanandhini, C. Simon, V. Pralong, Y. Breard, V. Caignaert, B. Raveau, P. Mandal, A. Sundaresan, and C. N. R. Rao, Zero magnetization in a disordered $(La_{1-x/2}Bi_{x/2})(Fe_{0.5}Cr_{0.5})O_3$ uncompensated weak ferromagnet, J. Phys.: Condens. Matter. **21**, 486002 (2009).

[38] B. Meng, Q. S. Fu, C. L. Li, X. H. Chen, Y. Qiu, and S. L. Yuan, Negative magnetisation and magnetic exchange interactions in Fe^{3+} substituted $Ca_2NdCr_2NbO_9$, Ceram. Int. **48**, 13108 (2022).

[39] L. Guo, Y. J. Bai, C. M. Huang, and W. L. Ma, Revisiting La_2MMnO_6 (M = Co, Ni, Cu, Zn) perovskites in view of $3d$-electron configuration, J. Appl. Phys. **124**, 065103 (2018).

[40] D. Mazumdar and I. Das, Role of $3d - 4f$ exchange interaction and local anti-site defects in the magnetic and magnetocaloric properties of double perovskite Ho_2CoMnO_6 compound, J. Appl. Phys. **129**, 063901 (2021).

[41] K. P. Patra and S. Ravi, Magnetic properties and exchange bias behavior in nanocrystalline $(Ho_{1-x}Sm_x)_2CoMnO_6$ ($x = 0$–0.5) double perovskite, J. Magn. Magn. Mater. **540**, 168476 (2021).

[42] L. T. Coutrim, D. Rigitano, C. Macchiutti, T. J. A. Mori, R. Lora-Serrano, E. Granado, E. Sadrollahi, F. J. Litterst, M. B. Fontes, E. Baggio-Saitovitch *et al.*, Zero-field-cooled exchange bias effect in phase-segregated $La_{2-x}A_xCoMnO_{6-\delta}$ (A = Ba, Ca, Sr; $x = 0, 0.5$), Phys. Rev. B **100**, 054428 (2019).

[43] S. Giri, M. Patra, and S. Majumdar, Exchange bias effect in alloys and compounds, J. Phys.: Condens. Matter **23**, 073201 (2011).

[44] R. L. Stamps, Mechanisms for exchange bias, J. Phys. D: Appl. Phys. **33**, R247 (2000).

[45] J. K. Murthy and A. Venimadhav, $4f - 3d$ exchange coupling induced exchange bias and field induced Hopkinson peak effects in Gd_2CoMnO_6, J. Alloy. Compd. **719**, 341 (2017).

[46] J. Nogues, D. Lederman, T. J. Moran, and I. K. Schuller, Positive Exchange Bias in FeF_2 – Fe Bilayers, Phys. Rev. Lett. **76**, 4624 (1996).

[47] J. Nogues, C. Leighton, and Ivan K. Schuller, Correlation between antiferromagnetic interface coupling and positive exchange bias, Phys. Rev. B **61**, 1315 (2000).

[48] Q. Y. Dong, K. Y. Hou, X. Q. Zhang, L. Su, L. C. Wang, Y. J. Ke, H. T. Yan, and Z. H. Cheng, Giant reversible magnetocaloric effect in antiferromagnetic rare-earth cobaltite $GdCoO_3$, J. Appl. Phys. **127**, 033904 (2020).

[49] A. A. Taskin and Y. Ando, Peculiar Ferrimagnetism Associated with Charge Order in Layered Perovskite $GdBaMn_2O_{5.0}$, Phys. Rev. Lett. **98**, 207201 (2007).

[50] L. Néel, Magnetic properties of ferrites: Ferrimagnetism and antiferromagnetism, Ann. Phys. Paris. **3**, 137 (1948).

[51] C. L. Li, T. Y. Yan, C. Chakrabarti, R. Zhang, X. H. Chen, Q. S. Fu, S. L. Yuan, and G. O. Barasa, Negative magnetization and the sign reversal of exchange bias field in $Co(Cr_{1-x}Mn_x)_2O_4$ ($0 \leqslant x \leqslant 0.6$), J. Appl. Phys. **123**, 093902 (2018).

[52] D. J. Webb, A. F. Marshall, A. M. Toxen, T. H. Geballe, and R. M. White, Observation of giant exchange anisotropy, IEEE Trans. Magn. **24**, 2013 (1988).

[53] Deepak, A. Kumar, and S. M. Yusuf, Intertwined magnetization and exchange bias reversals across compensation temperature in $YbCrO_3$ compound, Phys. Rev. Mater. **5**, 124402 (2021).

[54] R. P. Singh, C. V. Tomy, and A. K. Grover, Observation of tunable exchange bias in Sr_2YbRuO_6, Appl. Phys. Lett. **97**, 182505 (2010).

[55] F. Hong, Z. X. Cheng, J. L. Wang, X. L. Wang, and S. X. Dou, Positive and negative exchange bias effects in the simple perovskite manganite $NdMnO_3$, Appl. Phys. Lett. **101**, 102411 (2012).

[56] I. Fita, V. Markovich, A. S. Moskvin, A. Wisniewski, R. Puzniak, P. Iwanowski, C. Martin, A. Maignan, R. E. Carbonio, M. U. Gutowska *et al.*, Reversed exchange-bias effect associated with magnetization reversal in the weak ferrimagnet $LuFe_{0.5}Cr_{0.5}O_3$, Phys. Rev. B **97**, 104416 (2018).